PHYSICAL REVIEW A VOLUME 24, NUMBER 5 NOVEMBER 1981

Thermal relaxation in a dense liquid under shock compression

D. H. Tsai
National Bureau of Standards, Washington, D. C. 20234

S. F. Trevino
U.S. Army Armament Research and Development Command, Dover, New Jersey 07801
and National Bureau of Standards, Washington, D. C. 20234

(Received 1 June 1981)

We have studied by means of molecular dynamics the propagation of a planar shock wave in a dense, three-dimensional column of a simple modified Lennard-Jones liquid. The column is $49.37\sigma^2$ in cross section, and 238.5σ in length, where σ is the length parameter in the potential. The column contains approximately 10 000 atoms. It is initially in equilibrium at a density of $0.85\sigma^{-3}$ and temperature of $1.16\epsilon/k$, where ϵ is the energy parameter in the potential. Shock compression is effected by causing the column to move in the longitudinal direction with a velocity of $-U_p$ and to collide with its mirror image across a mirror located at the origin. From the motion of the atoms in response to this kind of excitation, we calculate the shock velocity and the shock-front structure in the liquid, as well as the profiles of mass density, stress distribution, and energy density behind the shock front. Our shock-front structure agrees well with that obtained from the Navier-Stokes equations, but we also find important differences between our shock profiles and those postulated or computed from the continuum theory. In particular, we find that in 4×10^{-11} s, the longest time of our calculations, the stress components did not relax to a hydrostatic condition, and the corresponding kinetic temperature profile showed a relaxation process similar to what we found earlier in a crystalline solid. We examine the atomistic mechanisms of the various relaxation processes, and discuss their implications on the shock compression of dense systems of solids and liquids as opposed to rarefied systems of gases.

I. INTRODUCTION

In previous work, we have reported[1-3] on our molecular-dynamical investigations of the shock-compression process in crystalline solids. The present work is a continuation of this line of investigation extended to a system of dense liquid. For crystalline solids, we found that under quite general conditions the thermal equilibration behind the shock front took place at a slower rate than the propagation of the shock front itself. We further identified the propagation of the thermally equilibrated region in the shock profile as longitudinal second sound generated by the shock-compression process, similar to the second sound generated by a displacement field.[4] Since the velocity of this longitudinal second sound is always lower than that of the longitudinal first sound (shock wave), we concluded that the equilibrated region would trail farther and farther behind the shock front, and that the kinetic temperature profile would change with time, i.e., the profile would be unsteady, even though the shock front itself has a steady velocity and a constant amplitude and width on average.

In our view, the physical basis for this slow thermal equilibration process (relative to the velocity of the shock wave) may be stated as follows: The shock front has a thickness of the order of 10 lattice planes. As it passes through the lattice, the atoms within the shock front are driven into large-amplitude, high-frequency oscillations, principally in the direction of shock-wave propagation. To reestablish thermal equilibrium, these oscillations must scatter and share their energies with other modes of lattice vibrations, so that an equilibrium *distribution* of oscillations may be established once again. In a dense system like a crystalline solid, this equilibration of energy is a slower process than the propagation of the shock (stress) wave. We believe that this process and the propagation of the equilibrium distribution behind the shock front are essentially similar to those encountered in the second-sound problem.[4-6] In both cases the controlling mechanism is the redistribution of kinetic and potential energies of the system by wave interaction, except in the shock compression we have large amplitude waves, and anharmonicity and dispersion are both important, whereas in the usual second-sound problem we have small amplitude waves which can be linearized, and dispersion is a small effect.

These results are not completely satisfactory for two reasons. First, our molecular-dynamical calculations are limited to relatively short times ($\sim10^{-10}$ s) and to macroscopically small systems ($\sim10^4$ atoms), by the sheer size of the computational problem. This is a difficulty we cannot do much to resolve because at this time we do not have the analytical tools to treat the fully anharmonic problem of shock compression in three di-

mensions, nor adequate computing power to push the numerical computation to longer times. Thus the long-time behavior of the energy-relaxation process is not altogether clear, despite advances in our understanding of the theoretical and physical bases of second sound in crystalline solids at low temperatures.

The second difficulty is that in addition to the energy-relaxation problem, there are other relaxation processes taking place in the shock profile, even in our model of a perfect lattice, so that the energy relaxation process is obscured. For example, in one case, we found that the model lattice was matastable in the uncompressed state, and that it underwent what may be considered as a phase transition during shock compression.[3] In other cases, we encountered instabilities in the structure of the compressed crystal[2] which buckled under shock loading. These phenomena are due to relaxation in the potential energy of the lattice, and are accompanied by stress relaxation. They undoubtedly take place also in a real solid, although in all likelihood by different mechanisms, e.g., by defect motion, dislocations, etc. Whatever the mechanism, relaxation of the potential energy clearly disturbs the kinetic energy in the relaxing region, and hence also the temperature of the system. This kind of detail, viz., structural rearrangement, further complicates the interpretation of the energy-relaxation process in the shock profile in our model calculations.

In an effort to develop further insight into these problems, we have carried out the present molecular-dynamical study of a simple, dense liquid under shock compression. Our objectives here are twofold: First, we wish to investigate the structural-relaxation process in the shock profile in the liquid. In particular, we would like to know if in the time of our molecular-dynamical calculations, the stresses in the shock profile are able to relax to a hydrostatic condition. This would give us some indication of the effect of the rate of strain on the structural relaxation in a simple liquid. In addition, since a simple liquid may be considered as the limiting case of a nonrigid solid, the results for the liquid should give the lower limit of the structural-relaxation time in a solid under similar conditions of shock compression. Second, if the structural-relaxation process in the liquid is sufficiently rapid ($\sim 10^{-11}$ s or shorter), we would then be able to focus attention on the energy-sharing process and study the problem of thermal relaxation behind the shock front. Actually, whether or not the structural- and thermal-relaxation processes can be clearly separated, we expect that the atomistic details in our model liquid will be useful for developing a clearer understanding of the dynamical processes which occur in dense systems driven far from equilibrium. These details are not available in the usual approach to continuum hydrodynamics (or mechanics) and they provide us with a valid and independent means for examining some of the basic assumptions employed in the continuum theory.

II. COMPUTATIONAL MODEL

Our model (Fig. 1) is similar to that described in Ref. 3. It is a column consisting of 36 blocks of 72 ($3\sqrt{2}\times 3\sqrt{2}\times 4$) fcc unit cells each. The [110], [1$\bar{1}$0], and [001] crystalline axes are aligned in the X, Y, and Z Cartesian directions, respectively, Z being the longitudinal direction of shock propagation. There are a total of 288 lattice sites in each block. We use the fcc lattice as a grid system and calculate the motion of the atoms with respect to the grid. We obtain the desired liquid density before compression by adjusting the size of the unit cells *and* the number of vacancies in each block. The atoms and the vacancies are free to move through the grid in response to thermal and mechanical agitation. When the temperature is sufficiently high, we are able to verify that the ensemble indeed takes on the structure of a liquid, as determined by its radial distribution function. For this study, we assigned ten vacancies to each block and adjusted the size of the unit cells to give a relative density before compression of $0.85\sigma^{-3}$, where σ is the length parameter in the Lennard-Jones potential which was used for this problem. At this density the column was $49.37\sigma^2$ in cross section and 238.5σ in length and contained about 10 000 atoms. The temperature before compression was set equal to $1.16\pm 0.03\epsilon/k$. Under these conditions, the uncompressed system was in the liquid state.[7]

Except at $Z=0$, we used cyclic boundary conditions to join these blocks together. Thus we represented a semi-infinite system by a liquid

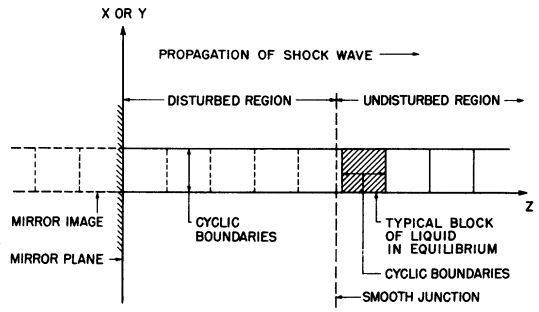

FIG. 1. Schematic model of the liquid column under shock compression.

column to a depth of 36 blocks. The column could, of course, be extended in the Z direction as desired. The plane at $Z=0$ where the shock compression began was constrained to be a stationary mirror plane. This plane contained a full array (no defects) of atoms fixed to their equilibrium fcc configuration. We generated the compression by causing the entire liquid column to move with a mass average velocity with respect to a stationary coordinate system of $U_c=-U_p$ in the Z direction toward the mirror plane, and to collide with its image moving with $+U_p$ from the other side of the mirror. Collision occurred at time $\tau=0$. The collision caused the mass average velocity along the liquid column progressively to come to a stop and this process generated a shock wave which propagated into the column. We have used two different initial conditions for U_c. In one case, for $\tau\geq 0$, we had

$$U_c=-U_p, \tag{1a}$$

where U_p was a constant. In the second case, we changed U_c from zero to $-U_p$ over a time interval τ_0 through a cosine relationship:

$$U_c=\begin{cases}-(U_p/2)[1-\cos(\pi\tau/\tau_0)] & \text{for } 0\leq\tau<\tau_0,\\ -U_p & \text{for } \tau\geq\tau_0.\end{cases} \tag{1b}$$

Condition (1a) simulated sudden start of compression, (1b) simulated gradual start of compression.

As the shock wave propagated into the uncompressed liquid column, the cyclic boundary conditions in the Z direction for the blocks affected by the shock wave were progressively removed, and beyond the shock front the disturbed region was required to join smoothly to the undisturbed region. In this way it was necessary to carry the equilibrium calculation ahead of the shock front for only one cyclic block of atoms, instead of for the entire length of the column. This scheme effected a considerable saving in computation, approaching 50% for a long column.

The interatomic potential was assumed to be the Lennard-Jones 12-6 potential (Eq. 2a). This potential was assumed to extend to an interatomic distance of $r=2.30\sigma$. Between $r=2.30\sigma$ and $r=2.4557\sigma$ (fifth-neighbor distance in the fcc lattice at zero pressure and zero temperature) we used an interpolation formula [Eq. (2b)] to join the Lennard-Jones potential smoothly to the $\Phi=0$ axis (continuous Φ and its first derivative):

$$\Phi_{LJ}=4\epsilon[(\sigma/r)^{12}-(\sigma/r)^{6}], \tag{2a}$$

$$\Phi_{INT}/2d^3C_{11}=AR^3+BR^2+CR+D, \tag{2b}$$

where

$$A=-0.0594173,$$

$$B=0.5443041,$$

$$C=-1.659962,$$

$$D=1.685161,$$

and $2d^3C_{11}=89.43\epsilon$ is the unit of energy, $R=r/d$, $d=r_1/\sqrt{2}=0.7766\sigma$, r_1 is the first-neighbor distance in the fcc lattice at zero pressure and zero temperature, and $C_{11}=95.47\epsilon\sigma^{-3}$ is the corresponding elastic constant in the [001] direction. We chose these units, rather than the simpler "natural" units of ϵ for energy, σ for length, etc., because we wished to express the shock velocity U_s and particle velocity U_p in terms of their Mach numbers based on the longitudinal [001] sound velocity $C_0=(C_{11}/\rho)^{1/2}$ through a crystalline solid at zero temperature and pressure. Then time is in units of d/C_0, force in units of $2d^2C_{11}$, mass in units of atomic mass m, and density in units of σ^{-3}. For argon, $\epsilon/k=120$ K, where k is Boltzmann's constant, and $\sigma=0.3405$ nm, $C_0=1494$ m/s, and $d/C_0=1.77\times10^{-13}$ s. We started the calculations with the liquid column already equilibrated at a given temperature and density, and imposed the initial and boundary conditions as described above to initiate the shock-compression process. We solved the Newtonian equations of motion for all the particles by an iterative Euler-Cauchy method.[8] Free movement of the atoms was allowed across cell boundaries, and in the course of such motion, the atoms would of course acquire different neighbors. To save computing time, we adapted the method of Streett *et al.*[9] to our iterative scheme as follows: We divided the neighbors of each atom into two groups. The inner group contained the first and second neighbors, the outer group contained the third, fourth, and fifth neighbors. For the first iteration at a given time step, the interactions between the atom of both the inner and outer groups of neighbors were calculated. For the second and subsequent iterations at this time step, we recalculated the interactions only of the inner group of neighbors and assumed that those of the outer group remained unchanged. This approximation should be good because with a small time step the displacement of any atom would be small, and hence the change in the interaction of the outer neighbors should be small also from one iteration to the next. The iterations were continued until the maximum change in position of all the atoms from one iteration to the next was smaller than a prescribed amount. Tests showed that the method of Streett *et al.* produced results in good agreement with those obtained by our earlier method by which we recalculated the interactions of both the

inner and the outer neighbors at each step of iteration. For example, in a system of 1200 atoms, the total energy of the system agreed to within 0.02% after 5 complete time steps, but the saving in computing time was by a factor of 30% by the method of Streett *et al.*

After the positions and velocities of all the atoms have been obtained, at each time step, we would then calculate from these such quantities as the potential and kinetic energies, mass density, stress components, etc., and their averages over distance and over time, and thus obtain a very detailed description of the shock profile. The calculation of these quantities will be described in Sec. III. But we should note two additional computational problems at this point. The first is the smooth junction between the disturbed and the undisturbed regions (Fig. 1). We required that the disturbance (mismatch) across this junction be no greater than the tolerance we prescribed on successive iteration. As the shock wave propagated into the undisturbed region, we would move the equilibrium block ahead of the shock front, and therefore the position of the smooth junction, by adding two lattice planes at a time on the far side and removing two planes on the shock-front side of this block. This scheme worked well most of the time. However, we found that the conditions at the junction of the two regions would occassionally drift away from the cyclic boundary conditions required for the equilibrium block of atoms. For example, mass diffusion in the disturbed region outside the cyclic block could sometimes be different from the mass diffusion at the corresponding point inside the block. We found that we could "repair" this kind of mismatch simply by moving the cyclic block farther ahead, and the computation would then continue without difficulty.

The second problem is that of energy conservation. Our numerical procedure solved Newton's equations of motion (force = mass × acceleration) for all the atoms, at discrete time intervals, to an accuracy of a few parts in 10^6. This procedure could not rigorously conserve the energy of the system. For example, in one run at $T_0 = 1.16\ \epsilon/k$, $\rho_0 = 0.85\sigma^{-3}$, and $U_p = 0.107$, the equilibrium block (278 atoms) showed a tendency to lose energy at an average rate of about 0.008% per time step ($\Delta\tau = 0.1$), as did the system (several thousand atoms) as a whole. A smaller time step would have conserved energy better, but would have also slowed down the computation. To correct for this energy nonconservation, we monitored the total energy of the equilibrium block, and kept it constant to within 1% by adjusting the kinetic energy of the atoms by a multiplicative factor as necessary. We applied a similar correction to the liquid in the shock profile except that in this case energy conservation must include the kinetic energy due to the mass average velocity of the liquid column before compression, as well as the PV work on the liquid as it flowed into the shock profile. Physically, this method of correction simulates the situation in which the liquid column is in close thermal contact with the surrounding liquid which is at the "correct" energy density. Our tests showed that the dynamics of the system was not appreciably altered when the energy correction was suppressed or applied. This point will be verified in Sec. III A. Instead of correcting for the energy nonconservation, we could have used the algorithm of LaBudde and Greenspan,[10] which was expressly designed to conserve energy. But this would be at the expense of not satisfying the equations of motion, at least not to the same degree as by our method. To our knowledge, the problems of numerical error in a large calculation involving thousands of particles are still not completely resolved. Further studies are needed before we can optimize the numerical method from the viewpoint of accuracy and efficiency.

III. RESULTS

We shall discuss the results of four specific cases. These are listed in Table I.

Figure 2 shows two three-dimensional plots of the shock-wave profiles of the mass density ρ and kinetic temperature E_k as functions of τ and Z for case A. In 200 units of time, the data cover about 240 "lattice planes" of distance in Z. The data have been smoothed by averaging over overlapping local regions. (See caption in Fig. 2 for a description of the averaging procedure.) The vertical scales are in arbitrary units. During this run we applied the energy correction discussed in the last section only to the uncompressed equilibrium block located well ahead of the shock front, but not to the shock profile itself. This accounts for the steady decrease of the average E_k in the shock profile, as may be seen in Fig. 2(b) when we compare the surface of E_k with the plane AOB which is at a constant height from the reference τ-Z plane. The effect of this energy nonconservation on the surface of mass density [Fig. 2(a)] is not quite so obvious, and we shall come back to this point in Fig. 4. But as we have mentioned earlier, we found that the energy correction did not affect the dynamical behavior of the shock profile very much (see Fig. 3). The qualitative features of the surfaces in Fig. 2 are therefore essentially correct. We now discuss the calcula-

TABLE I. Cases studied in this investigation.

Case	U_p [a]	Starting condition	Range of data	Energy correction applied to region: before compression	after compression
A	0.107	Eq. (1a)	$\tau=0$–200	Yes	No
B	0.107	Eq. (1b), $\tau_0=10$	$\tau=0$–150	Yes	No
C	0.107	Eq. (1b), $\tau_0=10$	$\tau=111.5$–150	Yes	Yes
D	0.213	Eq. (1a)	$\tau=0$–160	Yes	No

[a] The values of 0.107 and 0.213 for U_p are of no special significance. We had intended to make U_p equal to 0.1 and 0.2. However, on account of the adjustment of the unit-cell volume, necessary to give a mass density of $0.85\sigma^{-3}$, U_p acquired the values of 0.107 and 0.213, respectively.

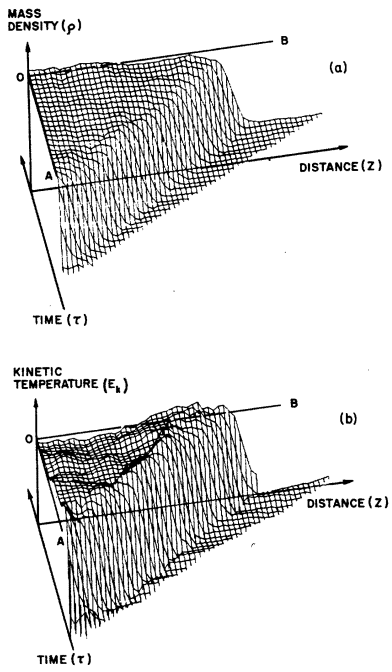

FIG. 2. Evolution of (a) mass density, ρ, and (b) kinetic temperature, E_k, as functions of time, τ, and distance, Z. The arrows on the axes indicate the direction in which the various quantities increase. The data correspond to case A of Table I. In both figures, the plane AOB is parallel to the τ-Z plane at an arbitrary height. It is provided as a guide for showing the steadiness attained in the shock profile. The data presented here are obtained from the computed results by means of an averaging procedure as follows. The averaged value of the function (here the mass density and kinetic temperature) at a point (τ, Z) is obtained by using all values of the function lying within a rectangle centered at the point (τ, Z) whose long axis is along the line connecting (τ, Z) and (τ_0, Z_0), the latter point being the point at which the shock front begins to develop. Values of the functions have been obtained in increments of τ of 0.5 and of Z of four averaged lattice planes. The dimensions of the rectangle are 20×10 in the above units everywhere except when the point is in the steep shock front in which case the dimensions are 20×3.

tions of the various quantities and the important dynamical results in detail. For convenience, we summarize the results in Table II. We also include the results of Hoover[11] for comparison.

A. Density profile and shock velocity U_s

We obtained the local mass (number) density by dividing the liquid column into contiguous volume segments and by counting the number of atoms in each segment. Figure 2(a) shows that the density profile surface, properly averaged, is a rather smooth surface. Figure 3(a) compares

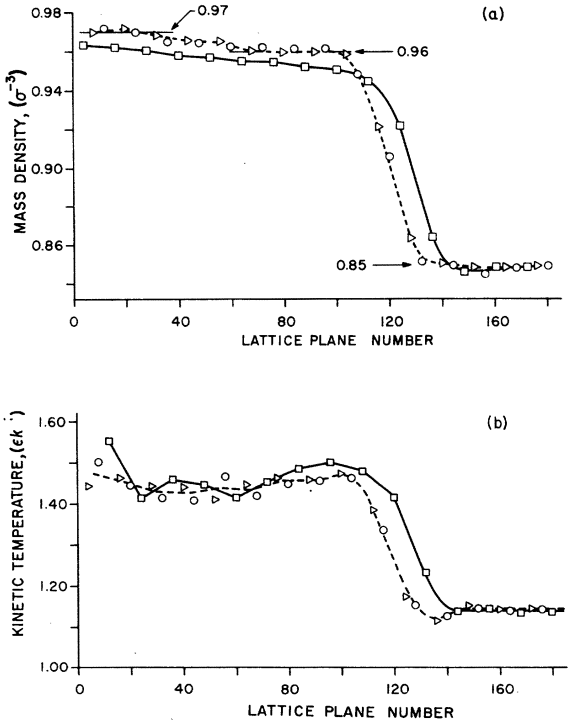

FIG. 3. Shock-wave profiles of mass density (a) and kinetic temperature (b) of case A: squares, case B: circles, and case C: triangles, at time step $\tau=150$. The data are averaged as described in the caption of Fig. 2. $\epsilon/k=120$ K for argon.

TABLE II. Summary of results.

Case	ρ_0	p_0	T_0	U_p	U_s	ρ_1	S_{xx}	T_1
A	0.85	3.18 ± 0.31 [a]	1.16 ± 0.03	0.107	0.90	0.95		
B	0.85	3.18	1.16	0.107	0.90	0.96		
C	0.85	3.18	1.16	0.107	0.90	0.96	10.45	
D	0.85	3.18	1.16	0.213	1.109	1.03	21.14 [b]	
Hoover	0.85	2.86 [a]	1.16	0.20	1.133	1.05	21.24	2.24

[a] Disagreement here is due to slight differences in the cutoff of the Lennard-Jones potential and in the treatment of the correction term beyond the cutoff. See Ref. 14.

[b] This value differs from the incorrect value of ~16 given in Ref. 15 in which the stresses in the shock profile were also incorrectly stated to be hydrostatic. See Sec. III B of text.

a section of that surface at $\tau = 150$ (case A) with the corresponding profiles in cases B and C. The horizontal scale is in lattice plane number. On this scale the distance between planes in the compressed region is not the same as that in the uncompressed region. Four points may be noted in these results. First, the shock front was farther ahead in case A (solid curve) than in B and C (dashed curve). This was due to the earlier start of full compression in case A. Second, behind the shock front the density profile for case A was everywhere lower than for B and C. The reason for this is not entirely clear. It might also be due to the sudden start of full compression in case A, resulting in a more pronounced elastic rebound of the liquid column (see Fig. 4) and a lower mass-density profile. Third, in cases B and C, the application of energy correction only to the region before compression (case B) or to the entire profile (case C) apparently made no appreciable difference in the mass-density profile. This is the basis of our statement that the dynamics of system was not appreciably altered by the omission of energy correction for the entire profile. Further evidence of this is given in Fig. 3(b) which shows that the corresponding kinetic temperature profiles for cases B and C are also essentially the same. In fact, the results for case A are also qualitatively and even quantitatively similar to those of cases B and C. Finally, the kinetic temperature [Fig. 3(b)] between zero and lattice plane 30 typically showed a tendency to rise toward the zeroth plane. This was due to the special mirror boundary condition at the zeroth plane, and the results in this region should not be included in the discussion of the dynamics of the shock profile. Excluding this region, we see that the kinetic temperature profiles in all three cases showed a tendency to rise from plane 30 to plane 100, before dropping steeply at the shock front. At the same time, the mass-density profiles showed a corresponding tendency to decrease over this distance. We show in Fig. 6 (case C) that the corresponding profiles of the stress components are uniform. Thus we conclude that the slight decrease in mass density, e.g., from 0.967 at plane 40 to 0.96 at plane 100 [Fig. 3(a)] was associated with the slight increase in the kinetic temperature (energy density) over this distance. We shall come back to this point when we discuss the problem of approach to equilibrium.

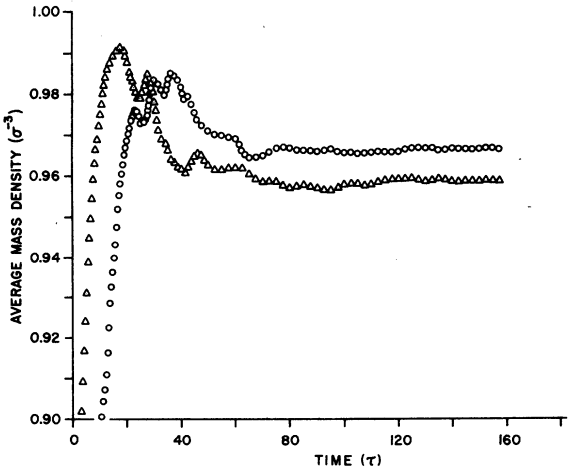

FIG. 4. Average mass density of the material behind the shock front as a function of time for case A: triangles, and cases B and C: circles. $\tau = 1.77 \times 10^{-13}$ s.

The difference in the start of compression [Eqs. (1a) and (1b)] also affected the response of the liquid column as a whole, as shown in Fig. 4. Here we have plotted the mass density averaged over the entire compressed region as a function of time for the three cases. With sudden start of compression (case A), the average mass density rose rapidly at first and approached an apparently steady value at $\tau \approx 100$ with an overshoot and some oscillations. With a gradual start of compression (cases B and C), the response was essentially the same, except the initial rise was more gradual, the overshoot was slightly less pronounced, and the approach to a steady value

occurred earlier, at $\tau \approx 80$. The response shown here may be considered as the damped elastic response of the liquid column to the kind of shock compression we imposed. It is likely that the difference in the rebound was responsible for the difference in the average values in the steady region in the three cases, but further work is required to establish this point. Note that it took a relatively long time ($\tau \approx 80$–100) for the initial transient to damp out. We shall return to this point later. At this time we conclude from Figs. 3 and 4 that the differences in the three cases, viz., the method employed in starting the compression and the application of energy correction in the numerical procedure, did not materially affect the dynamics of the shock-compression process. This conclusion was confirmed also by examination of the profiles of other quantities such as the stress components, energy density, etc.

Finally, we note that the propagation velocities of the shock front of all three profiles in Figs. 3 and 4 were steady on average for $\tau > 100$, after the average mass density has become steady. This steadiness may be seen qualitatively from Fig. 2(a) and along line LL in Fig. 8. Within the accuracy of the data, they all had the same value of $U_s = 0.90$.

Figure 5 shows the shock-front profile obtained by averaging the data of Fig. 2(a) (case A) between $\tau = 100$ and 200. The corresponding profile for $U_p = 0.213$ between $\tau = 100$ and 160 is also shown. The vertical scale is normalized to unity. The horizontal scale is now in units of σ. The zero of this latter scale is at the point (subscript zero) of the initial rise of the shock front. This point and the end point (subscript one), where the rise in density became very small, could be determined only approximately. This is an inherent difficulty in the determination of the thickness of the shock front. With this limitation in mind, we see that the shock-front profile for $U_p = 0.213$ was similar to the profile for $U_p = 0.107$, but was about 15% thinner. The corresponding density change differed by about a factor of 2.

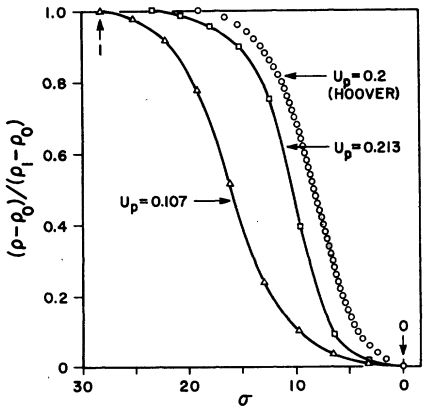

FIG. 5. Average mass-density profiles of the shock front at $U_p = 0.107$ and 0.213 (cases A and D). The profile calculated by Hoover (Ref. 11) for $U_p = 0.2$ is also shown. The value of zero for σ (distance) corresponds to the beginning of the shock front.

Recently Hoover[11] (see also Holian *et al.*[12]) has discussed the Navier-Stokes description of the shock-front structure in a Lennard-Jones liquid and has compared his continuum results with those obtained by Klimenko and Dremin[13] from molecular-dynamical calculations. Klimenko and Dremin apparently terminated their calculations rather early: Their results showed the shock front at 650 nm (65 Å). This corresponds to a run of about $\tau = 20$ in our time units. Thus their shock profile almost certainly could not have reached a steady state (see Fig. 4). Nevertheless, Hoover's results are in good quantitative agreement with Klimenko and Dremin's. Hoover has very kindly repeated his calculations under conditions which closely matched ours for $U_p = 0.213$. His density profile is compared with ours in Fig. 5. The agreement is again satisfactory, except for a small displacement in the horizontal direction due to the uncertainty in the point of initial rise in density. These results suggest that there is overall agreement between our calculations and those of Klimenko and Dremin. They also indicate that the characteristic sigmoidal shape of the shock front is not much affected by the steadiness of the shock profile as a whole, and only slightly affected by the rate of density change (rate of strain) across the shock front. We should emphasize again that our shock front (Fig. 5) was only smooth on average, and that within the shock-front thickness, there were large-amplitude, high-frequency interatomic oscillations.

With a steady mass-density profile of the shock front we can determine the mass average velocity of the liquid passing through the shock front from the condition of mass conservation, i.e.,

$$\rho(U_s - U') = \text{const} = \rho_0 U_s . \tag{3}$$

Here U_s is the velocity of the shock front and U' is the local mass average velocity of the liquid, both U_s and U' being measured in a coordinate system attached to the uncompressed liquid ahead of the shock front. In the present problem, this coordinate system moves with a velocity of $U_c = -U_p$ along the Z axis relative to the stationary laboratory coordinate system. If we denote by $U = U' - U_p$ the local mass average velocity of the liquid with respect to the stationary laboratory coordinates, then

$$U = U_s\left(1 - \frac{\rho_0}{\rho}\right) - U_p . \tag{4}$$

This is the local mass average velocity which must be considered in our calculation of the local kinetic temperature and the stress component S_{zz} in the shock profile. We shall take up these points later. At this time, we note that U (and also U'), in general, is a function of distance Z and time τ. Ahead of the shock front, $\rho = \rho_0$, therefore $U = -U_p$. Through the shock front U is given by Eq. (4) with ρ from Eq. (3) and Fig. 5. Behind the shock front, if $\rho = \rho_1$ for the entire profile, then $U = 0$. However, as Fig. 3(a) shows, ρ actually increased from about $0.96\sigma^{-3}$ behind the shock front by a small amount [~0.5% in Fig. 3(a), not considering the data between zero and plane 30] toward the tail of the shock profile. This change was due to the fact that the energy density in the shock profile was not uniform [Fig. 3(b)]: the higher the energy density, the lower the mass density. This was in the nature of thermal expansion, and its effect on U behind the shock front clearly would be small. We therefore assumed, for simplicity, that U was uniform and equal to zero behind the shock front in our calculation of the kinetic energy and S_{zz} profiles in that region.

B. Stress profile

We obtained the local stresses by imagining the liquid column to be cut by a number of planes normal to the X, Y, and Z axes, and by calculating the components of the interatomic forces and the components of the momentum flux intercepted by these planes. These components divided by the local areas then gave the local stress components. The details are given in Ref. 14. The planes over which the stresses were summed either must be stationary or moving at a uniform mass average velocity with respect to the reference coordinates. In the X and Y direction, the mass average velocities were zero both ahead and behind the shock front as well as through the shock front. In the Z direction, the mass average velocity was $-U_p$ ahead of the shock front, zero behind the shock front, and was equal to U [Eq. (4)] through the shock front. Since U must be obtained from the mass-density profile averaged over a large time interval, it was not convenient to calculate the instantaneous Z component of the momentum flux through the planes in the shock front while the computation was in progress. We therefore employed the relationship of momentum conservation, and obtained the average stress component S_{zz} through the shock front after the average profiles of ρ and U had been determined:

$$\Delta S_{zz} = S_{zz} - S_{zz0} = \rho_0 U_s (U + U_p) . \tag{5}$$

Figure 6 shows the stress profile (open symbols) obtained in this way for $U_p = 0.107$ at $\tau = 150$ (case C). The stress components in the uncompressed liquid were hydrostatic and these agreed quite well with those obtained in Ref. 14, shown at the extreme right around lattice plane 180. Through the shock front, as the liquid decelerated from $-U_p$ to zero mass average velocity, we found that S_{zz} [from Eq. (5)] was everywhere higher than S_{xx} and S_{yy}. This deceleration process clearly was a nonequilibrium process. Behind the shock front, we calculated S_{zz} by using the method of Ref. 14 and obtained a value of $10.45\epsilon\sigma^{-3}$, or $\Delta S_{zz} = 7.27\epsilon\sigma^{-3}$. This latter value agreed well with $\Delta S_{zz} = 7.32\epsilon\sigma^{-3}$ from Eq. (5), with $\rho_0 = 0.85$ and $U_s = 0.90$, showing that momentum was well conserved in our molecular-dynamical calculation. The individual stress components equilibrated rapidly in the longitudinal direction, showing that momentum equilibrium occurred with the velocity of shock-wave propagation. But S_{zz} remained different from S_{xx} and S_{yy} along the entire profile. This was found to be true also for case A, even at $\tau = 230$ or 4×10^{-11} s after the start of compression. The persistence of this nonhydrostatic state

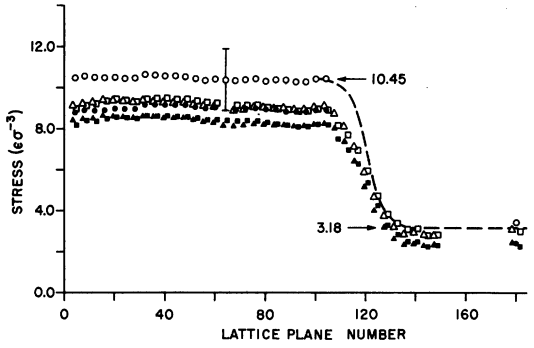

FIG. 6. Stress profile as a function of distance corresponding to time $\tau = 150$ for case C. The circles correspond to the stress in the Z direction (the direction in which the shock wave travels), and the triangles and squares to the stress in the X and Y directions, respectively. The open symbols give the values of the total stresses, the solid symbols give the values of the stresses due to the interatomic forces alone. The differences between the open and solid symbols represent the stresses due to momentum flux. The dashed curve for the total Z component of the stress is calculated from the density and mass-velocity profiles through the shock front. The data have been averaged as explained in the caption of Fig. 2. The vertical bar represents a typical value of one standard deviation obtained from the averaging procedure. The points at the extreme right at $\tau = 180$ are from Ref. 14 obtained under the same equilibrium conditions as those for the liquid column before compression.

of stress was rather surprising. To be sure, the difference between S_{zz} and S_{xx}, S_{yy} was not large and was within the typical local fluctuation (standard deviation, vertical bar in Fig. 6) of the data. Nevertheless, the anisotropy in stress was statistically significant. We were able to establish this point by investigating separately the contributions to the stress components by the interatomic forces and by the momentum flux. This may be seen also in Fig. 6 where we have plotted the stress components due to the interatomic forces, S_{xa}, S_{ya}, and S_{za} in solid symbols. The contributions due to the momentum flux are then represented by the difference between S_{xx} and S_{xa}, etc. Note that the momentum flux monitored here refers only to that part of the momentum carried by a subset of the fluid particles which moved across certain fixed planes in the fluid system during a given time interval. Its contribution to the stress component (averaged over time) was therefore not the same as the average kinetic energy (temperature) obtained from the corresponding velocity component of the ensemble (cf. Fig. 7). The difference between S_{za} and S_{xa}, S_{ya} shows the anisotropy in the atomic arrangement (structure) in the compressed region. Note also that the difference between S_{zz} and S_{xx}, S_{yy} was distributed about equally between that due to the anisotropy in the structure and that due to the anisotropy in the momentum fluxes.

We believe that the reason for this anisotropic behavior is as follows: The steady part of the compressed region for this case was at a stress (pressure) of $10.45\epsilon\sigma^{-3}$ or 0.438 GPa (4.38 kbar), temperature of $1.43\epsilon/k$ or 172 K, and density of $0.967\sigma^{-3}$. These conditions correspond very closely to the liquid density of argon at its freezing point at this pressure and temperature.[7] (The same was true for case D, except that the density of the compressed liquid was actually greater than the liquid density at its freezing point.) Thus our results suggested that the compressed region might be in the process of freezing. If so, it would be reasonable to identify the persistence of the nonhydrostatic stresses with the onset of solidlike behavior associated with freezing. Indeed a solid would be able to support nonhydrostatic stresses indefinitely. To establish this point more definitely, however, we should alter the condition of the liquid before compression so that its condition after compression would remain a liquid far from the freezing line. We plan to do these calculations in the future. Meanwhile, although these results are of great interest in themselves, we must admit that a part of our objective—that of shortening the structural-relaxation time with a liquid model—has not been satisfactorily accomplished.

C. Energy profile

In a classical system of particles in thermal equilibrium, the energy of the system satisfies the following conditions: (1) The energy density of the system is constant, (2) the time average of the kinetic energy E_k is also constant, (3) there is equipartition of E_k in the X, Y, and Z degrees of freedom, and (4) the velocity components of the thermal motion have a Maxwellian distribution. If the system can be represented as a coupled system of harmonic oscillators, then condition (3) also implies that there is equipartition of energy in the normal modes of the system. If in a local region the energy density and the average E_k change slowly with time, but conditions (3) and (4) are essentially satisfied, we have local thermal equilibrium. These considerations apply when the system (i.e., its center of mass) is either stationary or moving at a uniform velocity, but in the latter case E_k refers to the part of the kinetic energy associated with the thermal motion and not with the mass average velocity U. Thus

$$E_k=\frac{1}{2}\frac{m}{N}\sum_i[U_{xi}^2+U_{yi}^2+(U_{zi}-U)^2], \tag{6}$$

where m is the mass of the particles, U_x, U_y, and U_z the velocity components, U the local mass average velocity (here assumed to be in the Z direction), all referred to a stationary coordinate system. The summation in Eq. (6) is over the N particles of the system. The temperature T of the system is then related to E_k by

$$\tfrac{3}{2}kT=E_k. \tag{7}$$

In the case of a shock wave, through the thickness of the shock front U decelerates from $-U_p$ to zero over a very short distance, but the average profile of U is nevertheless steady, as Fig. 5 implies. We can gain some insight to the state of thermal equilibrium in this region by comparing the locally averaged kinetic energies associated with the velocity components. This is done in Fig. 7. Ahead of the shock front, the liquid column is in thermal equilibrium, and in this region E_{kx}, E_{ky}, and E_{kz} (the latter without the contribution from U^2) are the same. Within the shock front, while E_{kx} and E_{ky} remain approximately the same, E_{kz} is everywhere higher. Thus we see that in this region thermal equilibrium is clearly not obtained. These results are in qualitative agreement with those of Klimenko and Dremin.[11]

As the system emerges from the other side of the shock front, E_{kx}, E_{ky}, and E_{kz} appear to be the same once again, as in the uncompressed

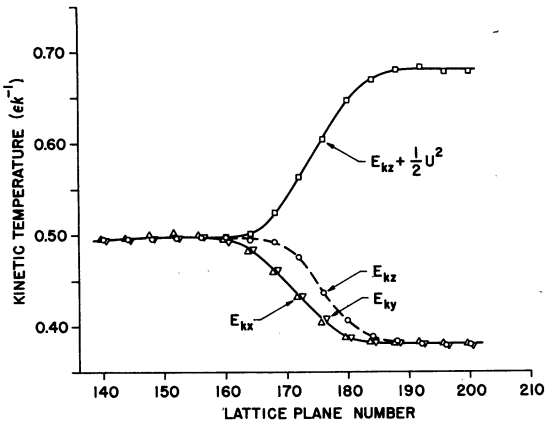

FIG. 7. Three components of kinetic temperature in the vicinity of the shock front for case A at time step $\tau = 200$. The Z component is given with and without the component due to mass average velocity. The data are averaged as described in the caption of Fig. 2. $\epsilon/k = 120$ K for argon.

liquid. The question now becomes: Is thermal equilibrium immediately reestablished following the shock front as is assumed in the continuum theory? If global thermal equilibrium is immediately reestablished then there should be no further energy relaxation between the shock front and the plane of impact (mirror plane), and we should observe a uniform temperature profile following the shock front. To answer this question, we again extend the calculations, as we did earlier with the crystalline solid, in order to allow the shock wave to propagate some distance from the mirror plane. We then simply observe the energy profile, along with the stress and mass-density profiles, to see if there is any evidence of energy relaxation. The kinetic temperature profiles obtained this way are shown in Figs. 8 and 9 for $U_p = 0.107$ (case A) and 0.213 (case D). The profiles in Fig. 8 are, of course, simply sections of the three-dimensional surface in Fig. 2(b).

We have already discussed the gradual decrease of the average height of the energy surface with increasing time in Figs. 2(b) and 3(b). This is also seen in Figs. 8 and 9. As has been pointed out, this energy decrease was due to energy nonconservation which, however, did not affect the dynamics of the shock wave to any appreciable extent. Thus we can use Fig. 8, for which we have the most extensive data, to discuss the energy-relaxation problem, even though for this case the total energy was not rigorously conserved. From our earlier results for the crystalline solid, we expect that the kinetic energy profile would exhibit an overshoot immediately behind the shock front. However, this was not observed in Fig. 8 at $\tau = 100$ and 120, which showed that the kinetic energy profile was nearly uniform. We believe that this was due to the transient effect mentioned in connection with Fig. 4 as well as the sudden compression at the mirror plane, and these combined to give a higher energy density near the mirror plane and to obscure the overshoot behind the shock front. With increasing time, the kinetic energy immediately behind the shock front remained nearly constant, but the tail portion of the profile began to decrease, so that by $\tau = 180$–200, the kinetic energy profile became rather similar to that for the crystalline solid. If we divide the shock profiles by line MM

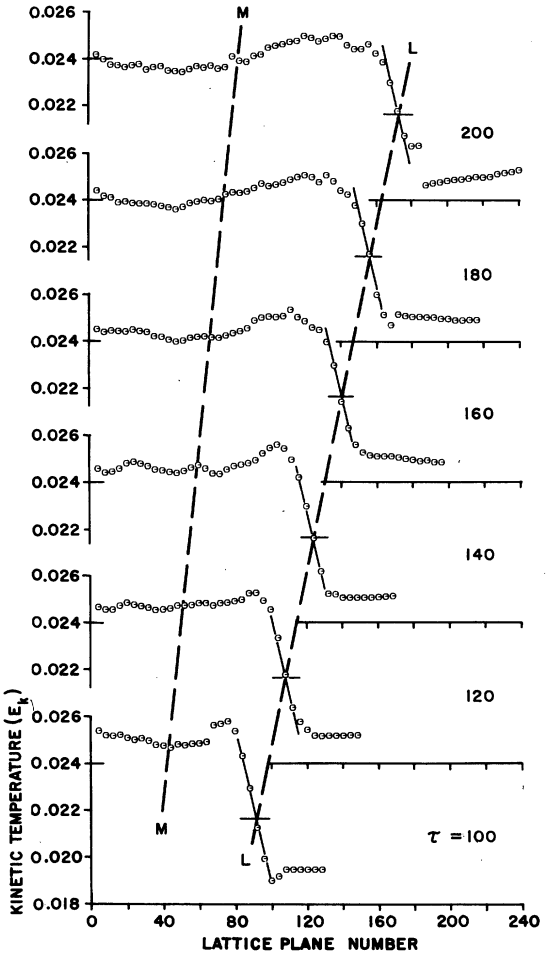

FIG. 8. Kinetic temperature E_k as a function of lattice plane number at various times τ for case A, $U_p = 0.107$, E_k is in units of $59.62\epsilon k^{-1}$. The line LL marks the progress of the shock front, and the line MM halfway between LL and the mirror plane, approximately distinguishes the relaxing region from the region in which thermal equilibrium is attained. The data are averaged in the same way as in Fig. 2. $\epsilon/k = 120$ K for argon.

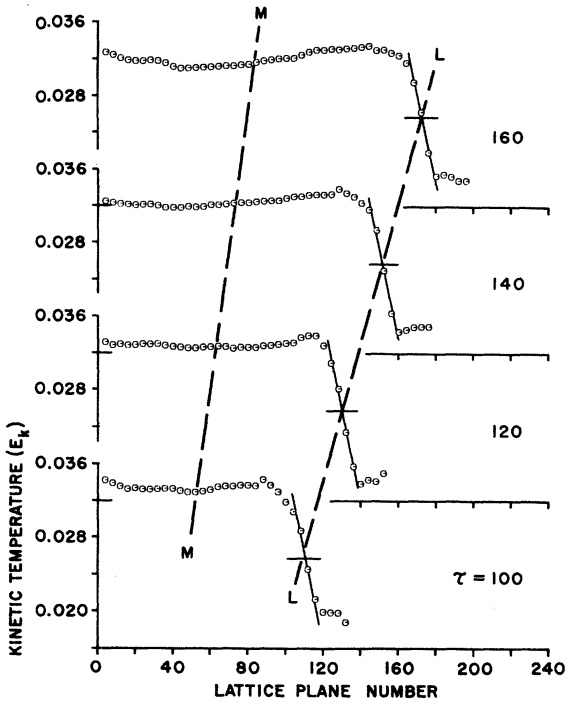

FIG. 9. Kinetic temperature E_k as a function of lattice plane number at various times τ for case D, $U_p = 0.213$. Other details are the same as in Fig. 8.

halfway between the shock front and the mirror plane, we see that *MM* approximately marks the beginning of the region in which the kinetic energy becomes relatively steady. At $\tau = 200$, the average kinetic energy in region *LM* behind the shock front is about 20% higher (measured from the uncompressed liquid) than in the tail portion of the profile. This then is the longitudinal thermal relaxation in the shock profile we have been discussing. In the present case of the liquid, it was superimposed on the relaxation of the transient associated with the compression process, and on the effect of the mirror boundary. The propagation velocity of *MM* is $0.5U_s$, again similar to what was obtained earlier for the crystalline solid. The kinetic energy profile is therefore unsteady behind the shock front in our liquid column, just as in a crystalline solid.

The above discussion applies in full to the data shown in Fig. 9 for $U_p = 0.213$, except here the results are more ambiguous because of the limited scope of the data. At $\tau = 160$, the average kinetic energy in region *LM* behind the shock front is about 15% higher than in the tail portion of the profile as we have shown in our earlier report.[15] The figure in that report is reproduced here as Fig. 10. It is the same as the corresponding figure in Fig. 9 except the data is averaged over

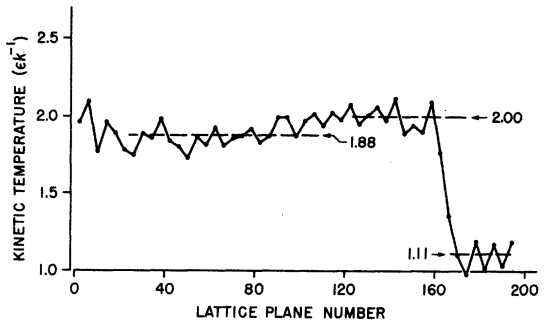

FIG. 10. Kinetic temperatures as a function of lattice plane number for case D at time step $\tau = 160$. The data are not so well averaged as those of Fig. 9. This figure is reproduced from Ref. 15. $\epsilon/k = 120$ K for argon.

a small interval of time.

We are not able at this time to give a concise and analytical description of the general nonequilibrium phenomena associated with the shock compression of a dense system, solid or liquid. However, we believe that many of the details of the shock profile in our liquid column, including the thermal-relaxation process behind the shock front, are analogous to what we have observed in the crystalline solid. We may give a qualitative description of these details as follows: As the steep shock front passes through the liquid, it drives the liquid within its narrow thickness into large-amplitude, high-frequency oscillations. These oscillations raise the energy density of the liquid, and they apparently do not thermalize immediately after the liquid emerges from the shock front, even though at this point E_{k_x}, E_{k_y}, and E_{k_z} are equal, as Fig. 7 shows. Our results indicate that thermal equilibration takes place at a rate considerably slower than the propagation of the shock front itself, and that the thermalization process also reduces the kinetic energy density. The junction between the relaxing region and the equilibrated region (line *MM* in Figs. 8 and 9) is not sharp, because as region *LM* relaxes toward its final state, local thermal equilibrium must be established at some point, especially if point *M* is at a large distance from the shock front. Thus there is some ambiguity in the precise location of line *MM*. However, over a large distance or a long-time interval, it is possible to establish that point *M* definitely moves at a lower velocity than the shock front at *L*, so that the kinetic energy-density profile is not steady. In close analogy to the case of the crystalline solid studied previously, we identify the propagation of this thermally equilibrated region as second sound in the liquid under shock compression.

Because of the close coupling between the kine-

tic energy and the potential energy in our dense system, we find that in the shock profile the region of high kinetic energy density is also the region of high potential energy density and high total (internal) energy density. The corresponding stress profile (Fig 6), in contrast, is uniform over the entire profile. Hence we expect that the mass-density profile would have to adjust so that the region of high energy density would correspond to the region of low mass density and *vice versa*. This is indeed the case, as we have already noted in Fig. 3(a).

IV. DISCUSSION

We have found that the thermal-relaxation process in the shock-wave profile in our dense liquid (and in crystalline solids) results from the redistribution of the kinetic *and* the potential energy of the system after it is driven out of equilibrium by a special kind of disturbance characteristic of the shock front. We may ask: What would be the thermal-relaxation process if the potential energy of the system was negligible compared with its kinetic energy, as in a rarefied system of monatomic gas particles? In such a system the equilibrium of energy by collision of the gas particles is quite efficient and is achieved within a few collisions in the shock front.[16] The kinetic temperature profile behind the shock front therefore is steady and uniform, i.e., in Figs. 8 and 9, *MM* would follow immediately after the shock front *LL* and would propagate with the same velocity. If the system is made up of complex gas molecules, then, as is well known also, the equilibration of energies among the translational, rotational, and internal degrees of freedom would require additional collisions among the molecules as well as among the internal vibrations within the molecules. The relaxation time then may be quite long compared with the rise time of the shock front. But this relaxation time remains constant on average because the molecules are of a finite size and have only a finite number of internal degrees of freedom. In this case, *MM* would lag behind *LL* by a constant distance and both would still have the same velocity, so that again the kinetic temperature profile would be steady and uniform. The stress profile would also be steady and uniform since momentum equilibration can take place with the velocity of the shock front and no "structural" relaxation is involved. These conditions are just those assumed in the continuum treatment of the dynamics of the shock wave. Hence we expect that if we were to calculate the molecular dynamics of the shock compression of a system of gas molecules, we would obtain results in full agreement with those obtained from the continuum model.

In a dense system of liquid or solid, the entire system may be considered to be a giant "molecule." As the shock front traverses this molecule, the part disturbed by the shock front and hence the number of "internal" degrees of freedom to be equilibrated increase linearly with time. This is the basic reason for the kind of relaxation process with an unsteady energy-density profile which we observe in dense systems. Our results show that the thermally equilibrated region propagates with the velocity of second sound. Even though we have only limited data from our calculations, we expect that the energy-density profile would remain unsteady as long as the propagation of the shock wave was maintained. Otherwise we must have some mechanism by which second sound can somehow increase its velocity to that of first sound. This kind of mechanism we are unable to postulate at this time. We note that in the liquid column studied here, the overshoot of the kinetic energy profile behind the shock front, is less pronounced than in the crystalline solid (cf. Ref. 3). In this sense, a simple liquid is intermediate between a crystalline solid and a simple gas, with the latter showing no thermal relaxation under shock compression.

These results, we emphasize, do not violate the conservation relations of mass, momentum, and energy across a *steady* shock front. They differ from the continuum results only in that the distributions of energy density and mass density follow the requirements of second-sound propagation, and are not steady and uniform as assumed in the Hugoniot conditions. The assumed uniform profiles would correspond to averaging the mass density and the energy density over the whole of the compressed region. These values are different from those in the equilibrated region in our relaxing profiles. For example, at $U_p = 0.107$ we obtain $U_s = 0.90$. If the profiles of mass density and energy density were uniform, we would have for the continuum model,

$$\rho_1 = \rho_0 U_s/(U_s - U_p) = 1.135\rho_0 ,$$

$$\Delta S_{xx} \approx P_1 - P_0 = \rho_0 U_s U_p = 7.32\epsilon\sigma^{-3} .$$

From our discrete model at the same U_p and U_s, the mass density in the equilibrated region is $1.138\rho_0$, and ΔS_{xx} is $7.27\epsilon\sigma^{-3}$. Comparing these data at the same density of $1.135\rho_0$, we estimate that ΔS_{xx} in the discrete model would be about $7.05\epsilon\sigma^{-3}$, or about 4% lower than $P_1 - P_0$ based on the continuum model. These results are consistent with those for the crystalline solid,[3] except in the liquid the difference in stress between the continuum model and the discrete model was

smaller.

There may, of course, be other relaxation processes, such as structural relaxation, taking place in the compressed region, as we have noted earlier. In solids there may be plastic flow, phase transition, etc. Even in our present liquid system, there should be further stress and structural relaxation from the nonhydrostatic condition. How these processes would affect the propagation of the shock wave and the equilibrium of energy behind the shock front remains to be investigated. But we expect that these processes would involve the relaxation and adjustment of the potential energy of the system and that they would be accompanied by further thermal relaxation to reach equilibrium. We note also that these processes cannot propagate faster than the shock front.

In the foregoing discussion, we referred to the characteristic profile of the shock front. By this we mean the narrow sigmoid shape (Fig. 5) with its steeply rising part extending the distance of only a few interparticle spacings. It is of interest to examine this point in greater detail. The shock compression of a one-dimensional chain with harmonic or anharmonic interactions extending to one or more neighbors has been extensively studied.[1,17] In this case the shape of the shock front can be clearly identified as due to the inertial effect of the mass of the atoms acted on by interatomic forces. In particular, the anharmonic forces tend to cause the shock front to steepen as it propagates. At the same time, the steepening process generates high-frequency components which propagate at lower velocities on account of dispersion. The sigmoid shape of the shock front results from a balance of these two effects, but the shape is steady only on average, and within the thickness of the shock front there are high-frequency, large-amplitude interparticle oscillations. If the forces are harmonic, then there is only the effect of dispersion, and the shock front in the shape of a step function will gradually become less steep as it propagates. But harmonic forces are not of interest here. The point of interest is that with any kind of reasonably realistic anharmonic forces, in the one-dimensional case, the steeply rising part of the shock-front profile always seems to be a few (5–10) lattice spacings thick. In fact, with anharmonic forces, we obtain essentially the same result for the shock-front profile in two- and three-dimensional crystalline solids, and in our three-dimensional liquid. On the basis of these results, we suggest that the shock front in these systems takes on its sigmoid shape because of the inertial and the anharmonic and dispersive effects in the system. This puts us in some conflict with the view, widely held in the continuum theory, that the finite shock-front thickness is due to the fact that there are viscous effects and thermal conduction within the shock front. This view encounters difficulties in the definition and the evaluation of the coefficients of viscosity and thermal conductivity under grossly nonequilibrium conditions within the shock front. Moreover, it fails to explain why our results show similar shock-front profiles in different dense systems in one, two, and three dimensions, in which the effects of viscosity and thermal conduction are surely altogether different.

There is by now a fairly large body of literature on molecular-dynamical studies of shock-wave propagation.[12,17–19] Although there is no general acceptance of our interpretation of the energy-relaxation process behind the shock front, the data produced by these studies are consistent. In our view, the different interpretations which have appeared in print thus far can be reconciled without too much difficulty. For example, Holian and Straub obtained unsteady shock profiles in various one-dimensional models,[12] and also in their three-dimensional solid under conditions of low shock strength. At high shock strength, characterized by a parameter $\alpha U_p > 1$, where α is the cubic anharmonic coefficient, they found a steady profile.[12] We do not have enough information from their report of 1979 to determine the mechanism of this transition from the unsteady to the steady shock profile. However, from the data presented, we suggest that they might be observing some kind of structural relaxation related to the stability of the lattice under compression, similar to what we have also observed.[2] Further work is needed to clarify this point. In Holian *et al.* (1980) on the shock-wave structure in a dense Lennard-Jones liquid,[12] they focused attention on the shock-front profile obtained from molecular dynamics and from the Navier-Stokes equations of continuum mechanics. The boundary conditions for their molecular-dynamical calculations were different from ours, but their results were generally similar to ours. In particular, they noted in their Fig. 9 that the velocity distributions behind the shock front showed a non-Maxwellian character and that the temperature behind the shock front was not immediately in equilibrium as postulated in the continuum theory. These results were also consistent with ours. However, their liquid column under shock compression was less than 25σ in length (comparable with Klimenko and Dremin's case[12]) at the end of their calculation. While this was long enough for establishing a steady shock-front profile, it was

probably not long enough for observing the features of thermal relaxation behind the shock front, as we have pointed out in Fig. 4.

Powell and Batteh[17] also have found unsteadiness in the shock profile in their one-dimensional model. They interpret their results on the basis of solitons or solitary waves which indeed do not thermalize rapidly, at least not with the velocity of the shock front. To the latter extent, our results agree. However, we should emphasize that in our three-dimensional models, liquid or solid, we do not observe any solitary waves in the shock profile trailing after the shock front.

With Paskin *et al.*,[19] our disagreement is with their method of calculating the kinetic energy profile. We have discussed this point in detail.[20] Briefly, their method suppresses the kinetic energy associated with the "planar" oscillations of the atomic planes behind the shock front. Since this is a part of the energy which must eventually thermalize and contribute to the energy of the shock-wave profile, we do not believe that they could exclude this contribution and still reach any sensible conclusion concerning the equilibration of temperature and the thermal-relaxation process behind the shock front. In our liquid column there is, in fact, no satisfactory way to define a unique planar velocity. If instead of the planar velocity Paskin *et al.* had used the mass average velocity [in Eq. (4)], which is the average velocity of the center of mass of the system averaged over time long compared with interatomic and/or interplanar oscillations, their results would have been in basic agreement with ours for crystalline solids.

Finally, we note that in the case of laminar collisionless shock waves in plasmas, it is known[21] that the *fluid* equations may have stationary solutions corresponding to solitary waves or nonstationary solutions in the form of infinite wave trains, i.e., there is no shock solution in the conventional sense with a steady shock profile. These results are qualitatively similar to those obtained by others and by us for the shock-wave propagation in dense systems of solids (and liquids), particularly in one dimension. In our view, this similarity exists, despite the vast differences in the forces in the plasma and in the solid/liquid systems and in the interparticle spacing, because the coupling of the particles and hence the mechanism of energy sharing in these systems are basically similar: In the dense solid/liquid, energy sharing occurs through the coupling of the atoms via the interatomic potential, as we have seen in our discussion; in the collisionless plasma, energy sharing occurs in an analogous manner through the coupling of the charged particles via the surrounding electromagnetic fields. Apart from its intrinsic scientific interest, the reason for mentioning collisionless shock waves in plasma is that it may actually be simpler to make experimental measurements on the plasma system, for example, the bow wave of the earth in the solar wind, than on the dense system of solid or liquid. It constitutes an alternative way to study the energy-sharing problem in a coupled, many-body system.

In the foregoing, we have pointed out a number of features in our results which are in agreement or are consistent with those obtained by other investigators of the shock-wave problem. This kind of general agreement notwithstanding, the real test of the success or failure of our model and of the results accumulated thus far clearly must be judged by direct comparison with the measured temperature profiles from shock-wave experiments. Only then can we expect to achieve a more satisfactory and more complete understanding of this interesting problem.

ACKNOWLEDGMENTS

We thank R. D. Mountain for several illuminating discussions. We also thank the Reactor Radiation Division of the Center for Material Science, National Measurement Laboratory, National Bureau of Standards, for the use of the VAX 11/780 computer. Their efficient management of this computing system has contributed in important ways to the successful completion of our massive computational work. This project was supported in part by the Army Research Office under Contract MIPR No. ARO 2-79.

[1]D. H. Tsai and C. W. Beckett, J. Geophys. Res. 71, 2601 (1966); in *Behaviour of Dense Media under High Dynamic Pressures, Symposium HDP, International Union of Theoretical and Applied Mechanics (IUTAM), Paris, Sept. 1967* (Gordon and Breach, New York, 1968), pp. 99–108; D. H. Tsai, in *Accurate Characterization of the High-Pressure Environment*, edited by E. C. Lloyd (Natl. Bur. Stand. Spec. Pub. 326, Washington, D. C., 1971), pp. 105–123; D. H. Tsai and R. A. MacDonald, J. Phys. C 6, L171 (1973).

[2]D. H. Tsai and R. A. MacDonald, High Temp.–High Pressures 8, 403 (1976).

[3]R. A. MacDonald and D. H. Tsai, Phys. Rep. 46, 1 (1978).

[4]P. C. Kwok and P. C. Martin, Phys. Rev. 142, 495 (1966); L. Sham, *ibid.* 156, 494 (1967); 163, 401 (1967).

[5]J. C. Ward and J. Wilks, Philos. Mag. 43, 48 (1952); E. W. Prohofsky and J. A. Krumhansl, Phys. Rev. 133, A1403 (1964); R. A. Guyer and J. A. Krumhansl, *ibid.* 133, A1411 (1964); Phys. Rev. 148, 766 (1966).

[6]C. C. Ackerman, B. Bertman, H. A. Fairbank, and R. A. Guyer, Phys. Rev. Lett. 16, 789 (1966); C. C. Ackerman and W. C. Overton, *ibid.* 22, 764 (1969); T. F. McNelly *et al.*, *ibid.* 24, 100 (1970); V. Narayanamurti and R. C. Dynes, *ibid.* 28, 1461 (1972).

[7]J.-P. Hansen and L. Verlet, Phys. Rev. 184, 151 (1969).

[8]L. Collatz, *The Numerical Treatment of Differential Equations*, 3rd ed. (Springer, Berlin, 1960), p. 54.

[9]W. B. Streett, D. J. Tildesley, and G. Saville, Mol. Phys. 35, 639 (1978).

[10]R. A. LaBudde and D. Greenspan, J. Comp. Phys. 54, 134 (1974).

[11]W. G. Hoover, Phys. Rev. Lett. 42, 1531 (1979).

[12]B. L. Holian and G. K. Straub, Phys. Rev. B 18, 1593 (1978); G. K. Straub, B. L. Holian, and R. G. Petschek, *ibid.* 19, 4049 (1979); B. L. Holian and G. K. Straub, Phys. Rev. Lett. 43, 1598 (1979); B. L. Holian, W. G. Hoover, B. Moran, and G. K. Straub, Phys. Rev. A 22, 2798 (1980).

[13]V. Y. Klimenko and A. N. Dremin, in *Detonatsiya, Chernogolovka*, edited by O. N. Breusov *et al.* (Akad. Nauk, Moscow, 1978), p. 79.

[14]D. H. Tsai, J. Chem. Phys. 70, 1375 (1979).

[15]D. H. Tsai and S. F. Trevino, in *High-Pressure and Technology, Proceedings of the Seventh International Conference of the International Association for the Advancement of High-Pressure Science and Technology (AIRAPT), LeCreusot, France, July 30–Aug. 3, 1979*, edited by B. Vodar and Ph. Marteau (Pergamon, Oxford, 1980), Vol. 2, pp. 1051–1053.

[16]See, for example, G. N. Patterson, *Molecular Flow of Gases* (Wiley, New York, 1956), Chap. 4.

[17]R. Manvi, G. E. Duvall, and S. C. Lowell, Int. J. Mech. Sci. 11, 1 (1969); R. Manvi and G. E. Duvall, J. Phys. D 2, 1389 (1969); G. E. Duvall, R. Manvi, and S. C. Lowell, J. Appl. Phys. 40, 3771 (1969); J. Tasi, *ibid.* 43, 4016 (1972); 44, 1414 (1973); J. H. Batteh and J. D. Powell, *ibid.* 49, 3933 (1978); J. Tasi, *ibid.* 51, 5804 (1980).

[18]P. K. Salzman, A. F. Collings, and C. J. Pings, J. Chem. Phys. 50, 935 (1969); K. Niki and S. Ono, Phys. Lett. 62A, 427 (1977).

[19]A. Paskin and G. J. Dienes, J. Appl. Phys. 43, 1605 (1972); A. Paskin and G. J. Dienes, Solid State Commun. 17, 197 (1975); A. Paskin, A. Gohar, and G. J. Dienes, J. Phys. C 10, L563 (1977); A. Paskin, A. Gohar, and G. J. Dienes, J. Phys. Chem. Solids 39, 1307 (1978); A. Paskin, A. Gohar, and G. J. Dienes, J. Phys. C 11, L857 (1978).

[20]D. H. Tsai and R. A. MacDonald, J. Phys. C 11, L365 (1978).

[21]See, for example, D. A. Tidman and N. A. Krall, *Shock Waves in Collisionless Plasmas* (Wiley-Interscience, New York, 1971), Chaps. 1, 2, and 5; C. K. Chu and R. A. Cross, in *Advances in Plasma Physics*, edited by A. Simon and W. B. Thompson (Wiley-Interscience, New York, 1969), Vol. 2, pp. 139–202.